

Delayed Enrichment by Unseen Galaxies: Explaining the Rapid Rise in IGM CIV Absorption from $z = 6-5$

R. H. Kramer ^{*1}, Z. Haiman ^{†2}, and P. Madau ^{‡3}

¹ *Institute for Astronomy, ETH Zurich, Wolfgang-Pauli-Strasse 27, CH-8093 Zurich, Switzerland*

² *Department of Astronomy, Columbia University, 550 West 120th Street, New York, NY 10027, USA*

³ *Department of Astronomy and Astrophysics, University of California Santa Cruz, 1156 High Street Santa Cruz, CA 95064, USA*

ABSTRACT

In the near future, measurements of metal absorption features in the intergalactic medium (IGM) will become an important constraint on models of the formation and evolution of the earliest galaxies, the properties of the first stars, and the reionization and enrichment of the IGM. The first measurement of a metal abundance in the IGM at a redshift approaching the epoch of reionization already offers intriguing hints. Between $z = 5.8$ and 4.7 (a 0.3 Gyr interval only 1 Gyr after the big bang), the measured density of CIV absorbers in the IGM increased by a factor of ~ 3.5 (Ryan-Weber et al. 2009; Becker, Rauch & Sargent 2009). If these values prove to be accurate, they pose two puzzles. (1) The total amount of CIV at $z = 5.8$ implies too little star formation to reionize the IGM by $z = 6$ or to match the *WMAP* electron scattering optical depth (τ). (2) The rapid growth from $z \approx 6-5$ is faster than the buildup of stellar mass or the increase in the star formation rate density over the same interval. We show that a delay of $\sim 0.5-0.7$ Gyr between the instantaneous production of ionizing photons and the later production of metal absorption features (added to the delay due to stellar lifetimes) can provide the full explanation for both puzzles. We calculate the delay in metal production due to finite stellar lifetimes alone and find that it is too short (~ 0.2 Gyr) to explain the rapid evolution. The additional delay could naturally be explained as the result of ~ 100 km/s outflows carrying carbon to distances of $\sim 50-70$ kpc, the typical distance between galaxies and CIV absorbers in enrichment simulations (Oppenheimer, Davé & Finlator 2009; Cen & Chisari 2010).

Key words: galaxies: formation – galaxies: high-redshift – intergalactic medium – cosmology: theory – quasars: absorption lines – dark ages, reionization, first stars.

1 INTRODUCTION

Most of the star formation taking place during the reionization epoch remains invisible to current observations, and a large fraction may remain invisible even to the *James Webb Space Telescope (JWST)* (e.g. Salvaterra, Ferrara & Dayal 2010). This unobserved population of faint galaxies must contribute most of the high-energy photons that reionized the intergalactic medium (IGM). The ionization state of the intergalactic medium is one important probe of this population. Other constraints are provided by the detection of luminous Lyman-break galaxies (LBGs) and Lyman- α emitters (LAEs) at $z > 6$ (e.g. Bouwens et al. 2010; Tilvi et al. 2010). Although the directly observed population cannot account for all of the photons necessary to reionize the IGM

(and especially to match the *WMAP* Thompson-scattering optical depth from free electrons τ , Bolton & Haehnelt 2007; Oesch et al. 2009), they constrain the high-luminosity end of the galaxy luminosity function (LF).

The distribution (by element, in time, and in space) of the elements synthesised in these early generations of stars and subsequently expelled into the IGM (or incorporated into low-mass stars still observable in the local universe) will become an important source of information about the epoch of reionization in the near future. Currently the highest-redshift measurements of metal abundance in the IGM come from searches for CIV absorption features in quasar spectra (Ryan-Weber et al. 2009; Becker, Rauch & Sargent 2009).

The uncertainty on the $z \gtrsim 5$ CIV measurements is still large, but if they prove to be accurate then, taken at face value, they represent two puzzles. (1) Ryan-Weber et al. (2009) find that the total amount of CIV at $z = 5.8$ implies too little star formation to reionize the IGM by $z = 6$. (2) Becker et al. (2009) find that the fractional increase in CIV

* Zwicky Fellow, ETH Zurich, roban.kramer@phys.ethz.ch

† zoltan@astro.columbia.edu

‡ pmadau@ucolick.org

density is larger than either the buildup of stellar mass or the increase in the star formation rate density (SFRD) over the same interval.

We show here that both puzzles can be solved by a delay between the production of ionizing photons and the enrichment of the IGM with the associated metals. Indeed, this paper is motivated by the fact that such a delay is inevitable, since a significant fraction of the carbon output of a stellar population is produced by long-lived, intermediate-mass stars. In the next section (§2), we discuss current observations and models of C IV in the IGM in more detail. Section 3 presents our simple framework for modelling reionization and enrichment based on a galaxy luminosity function history. In Section 4 we show that we can match reionization (§4.1) and enrichment constraints at a single redshift (§4.2) with simple models and physically plausible parameters, then go on to show that a delay of 0.5–0.7 Gyr (in addition to the delay due to finite stellar lifetimes) can produce the observed rapid rise in C IV absorber density (§4.3). In section 5 we summarise our results and briefly mention how future observations and models will improve our understanding of early metal enrichment and reionization.

2 EXISTING OBSERVATIONS AND MODELS

Observations of absorption features in high-redshift quasar spectra are beginning to probe the IGM metallicity at redshifts approaching $z = 6$ (arguably close to the final stages of reionization). Currently the highest-redshift measurements are of the C IV 1548.2, 1550.8 Å doublet, redshifted into the near infrared (NIR). Ryan-Weber et al. (2009) identified three (plus one tentative) C IV features in a search between $z = 5.2$ and 6.2 along lines of sight to 9 quasars with a combined absorption distance of $\Delta X = 25.1$.¹ Becker et al. (2009) performed a similar search in four sight lines ($\Delta X = 11.3$), finding no absorption features. This is particularly surprising since their observations were sensitive to even lower column densities than Ryan-Weber et al. (2009), and therefore would have been expected to detect more C IV features per unit absorption distance if the column-density distribution followed the declining power-law form found at lower redshift.

Converting the absorption feature detections to the average C IV density in the IGM (expressed as a fraction of the critical density), and correcting for their completeness limits in column density, Ryan-Weber et al. (2009) found

$$\Omega_{\text{C IV}}(\langle z \rangle = 5.76) = (5.0 \pm 3.0) \times 10^{-9}. \quad (1)$$

Applying similar corrections to observations by Pettini et al. (2003), they found

$$\Omega_{\text{C IV}}(\langle z \rangle = 4.69) = (17 \pm 6) \times 10^{-9}. \quad (2)$$

The errors are still large on these measurements. If the $z = 5.76$ value is revised toward the upper end of the allowed range, then the puzzle of the rapid evolution in C IV will go away. However we will proceed here under the assumption

¹ ΔX is defined so that objects with constant comoving density and physical cross section have constant density per unit ΔX (Tyson 1988; Ryan-Weber et al. 2009).

that the central values are essentially correct, and therefore seek to resolve the puzzle of the rapid C IV growth.

The C IV density in the IGM is approximately constant at $\Omega_{\text{C IV}} \sim 2 \times 10^{-8}$ from $z = 2$ –4 (Ryan-Weber et al. 2009; Songaila 2001), a surprising result given that this is a period of intense star formation. Models of IGM enrichment have successfully explained this as the result of a decreasing fraction of carbon in the triply-ionized state, offsetting the concurrent rise in total carbon density (Oppenheimer & Davé 2006; Davé & Oppenheimer 2007; Oppenheimer & Davé 2008).

Models of enrichment and carbon ionization at $z > 4$ are able to produce a rise in $\Omega_{\text{C IV}}$ between $z = 6$ and 5 consistent with the observations (Oppenheimer, Davé & Finlator 2009; Cen & Chisari 2010), at least within their large uncertainties. Both (Oppenheimer et al. 2009) and (Cen & Chisari 2010) find that the total amount of carbon in the IGM increases by a factor of 2.5 to 3 in this interval, while the fraction of carbon in the triply-ionized state only increases by a factor of $\lesssim 1.25$.

These simulations do not self-consistently model reionization, so they are unable to directly elucidate the relationship between reionization and enrichment, which is our primary concern here. We are therefore interested in investigating the connections between reionization, enrichment, and the population of galaxies responsible for both.

3 METHODS

3.1 Connecting Reionization and the Galaxy Luminosity Function

In order to answer the above questions, we need to model the luminosity function of galaxies, and from that calculate the total ionizing emissivity as a function of redshift. We assume the LF is a Schechter function. Observations suggest that ϕ_* (the density normalisation) and α (the faint-end slope of the LF) are approximately constant from $z = 4$ to 6 (Bouwens et al. 2007). Neither are constrained as precisely at higher redshift, but Bouwens et al. (2010) find that the observed LF at $z = 7$ and 8 is consistent with constant α and ϕ_* , though the maximum-likelihood values move toward steeper faint-end slopes ($\alpha = -1.94 \pm 0.24$ at $z \sim 7$ and -2.00 ± 0.33 at $z \sim 8$). We therefore parametrise the evolution of the LF by varying only M_* with redshift. At $z < 9.0$ we use the M_* values from Bouwens et al. (2008), linearly interpolated as a function of redshift. At $z > 9$ we assume M_* is linear in redshift with slope β_{M_*} . The parameters α and β_{M_*} therefore control the extrapolation of the LF to lower luminosities and higher redshifts than have yet been probed by observations.

To convert the observed LF to an ionizing photon emissivity (or rate density, photons⁻¹ s⁻¹ Mpc³), we use the Bolton & Haehnelt (2007) spectral energy distribution (SED) and an escape fraction $f_{\text{esc}\gamma}$. With this SED, the ratio of ionizing photon production rate to UV luminosity is $\dot{N}/L(1500 \text{ \AA}) = 8.4 \times 10^{24}$ photons s⁻¹/(erg s⁻¹ Hz⁻¹), though we assume only a fraction $f_{\text{esc}\gamma}$ of these escape into

the IGM.² With these factors we convert the integrated LF history into an ionizing emissivity history, and then into the ionized fraction of the IGM $x(z)$. We ignore twice ionized helium, and assume that once-ionized helium has the same number fraction as hydrogen, and include recombinations. Recombinations are calculated with clumping factor $C \equiv \langle n_{\text{HII}}^2 \rangle / \langle n_{\text{HII}} \rangle^2 = 4$ (see §4.1 for discussion of varying C), gas temperature 10^4 K (giving case B recombination rate $\alpha_B = 2.6 \times 10^{-13} \text{ cm}^3 \text{ s}^{-1}$, Hui & Gnedin 1997) and assuming all ionized gas is contained in fully ionized bubbles. We integrate the LF down to $M_{\text{AB}}(UV) = -13.04$, equivalent to a star formation rate of $0.01 m_{\odot}/\text{yr}$ (Kennicutt 1998; Oesch et al. 2009). We use the “WMAP7 + BAO + H0” mean cosmological parameters from Komatsu et al. (2010) throughout this paper.³ The values of $f_{\text{esc}\gamma}$, β_{M*} , and α are discussed in §4.

3.2 Connecting Reionization and Carbon Production

We define $f_{x\text{CIV}}$ as the ratio between the total rate (with no delay) of CIV production and the total rate of ionizing photon production, so that:

$$\dot{\Omega}_{\text{CIVinst}}(z) = \dot{x}_{\text{total}}(z) f_{x\text{CIV}}, \quad (3)$$

where $\dot{\Omega}_{\text{CIVinst}}(z)$ would be the rate of CIV density increase with no delay in emission, and $\dot{x}_{\text{total}}(z)$ is the ratio of the total rate density of ionizing photon production to the total number density of hydrogen and helium atoms.

The $f_{x\text{CIV}}$ ratio depends on a number of factors:

$$f_{x\text{CIV}} = \left[\frac{f_{\text{CIV}} f_{\text{esc}Z}}{r_{\gamma Z}} \right] (X_C/Z) \Omega_{\text{baryon}}. \quad (4)$$

The fraction of all metal mass in carbon is $X_C/Z = 0.178$ (the solar value from Asplund, Grevesse & Sauval 2005). $\Omega_{\text{baryon}} = 0.0456$ is the fraction of the critical density contributed by baryons (Komatsu et al. 2010). The terms in square brackets (the fraction of carbon in CIV, f_{CIV} ; the fraction of metals that escape galaxies, $f_{\text{esc}Z}$; and the ratio of metal nucleon to ionizing photon production, $r_{\gamma Z}$) are highly uncertain. We use the representative values of $f_{\text{CIV}} = 0.5$ (the maximum theoretical value, see Ryan-Weber et al. 2009; Songaila 2001) and $f_{\text{esc}Z} = 0.2$ (equal to our fiducial $f_{\text{esc}\gamma}$), and emphasise that it is only the product of these uncertain factors that matters.

The ratio of ionizing photons to metal nucleons produced by a stellar population can be expressed as

$$r_{\gamma Z} = \eta \frac{E_p}{E_{\text{avg}}}, \quad (5)$$

where η is the ratio of total ionizing photon energy to total rest-mass energy of the metals produced in a stellar population, E_p is the rest-mass energy of a proton, and E_{avg} is

² Note that $\dot{N}/L(1500 \text{ \AA})$ is sensitive to the initial mass function and metallicity of the stellar population, though we ignore this dependence here. $\dot{N}/L(1500 \text{ \AA})$ is completely degenerate with $f_{\text{esc}\gamma}$ in our formalism.

³ Cosmological calculations were performed with the COSMOLOGY python package, version 0.1, available at <http://roban.github.com/CosmoLoPy/>.

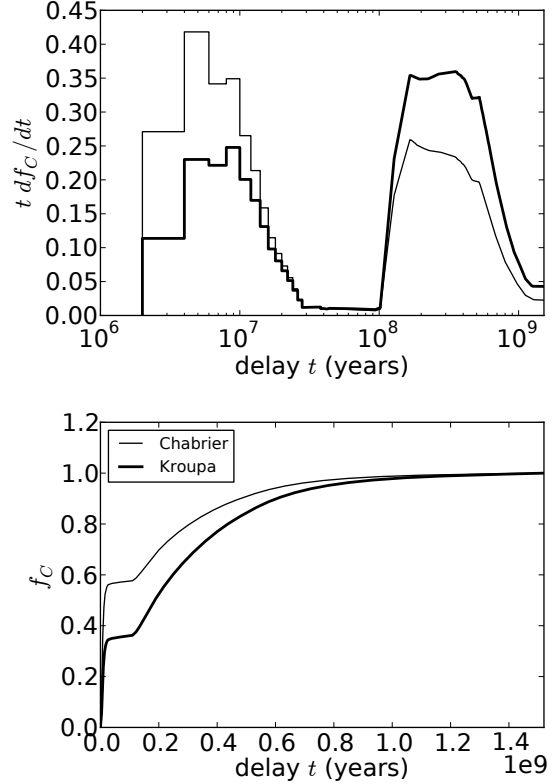


Figure 1. Delay functions for carbon production. Differential (top panel) and cumulative (bottom panel), delays are calculated with Chabrier (thin curve) and Kroupa (thick curve) IMFs. The differential delay is shown on a logarithmic time scale, while the cumulative delay is shown on a linear time scale. Note the rapid emission from supernovae ($\sim 10^7$ years) and the longer tail from AGB stars (\sim a few $\times 10^8$ years).

mean energy of ionizing photons (Schaerer 2002). For a stellar population with $Z = 1/50 Z_{\odot}$, Schaerer (2002) calculate $\eta = 0.014$ and $E_{\text{avg}} = 21.95 \text{ eV}$, yielding $f_{x\text{CIV}} = 1.4 \times 10^{-9}$. Note that this η value does not include yields from low- and intermediate-mass stars (LIMS, $m < 8 m_{\odot}$), stellar wind mass loss, or Type I SN contributions, all of which would decrease η (and increase the enrichment to ionization ratio $f_{x\text{CIV}}$). We will also explore scenarios using the solar-metallicity ($Z = Z_{\odot}$) values of $\eta = 0.0036$ and $E_{\text{avg}} = 20.84 \text{ eV}$ (calculated with mass loss and SN Ibc, but still without LIMS), resulting in $f_{x\text{CIV}} = 5.0 \times 10^{-9}$.

Changing the M_* vs. z slope (β_{M*}) or the faint-end slope of the LF (α) changes both the ionization and enrichment histories. Changing $f_{\text{esc}\gamma}$ only affects the ionization history. Changing $f_{x\text{CIV}}$ only affects the enrichment history.

3.3 The Carbon Delay Distribution Due to Stellar Lifetimes

Carbon is not produced instantly upon formation of a population of stars, unlike, for our purposes, ionizing photons. Instead carbon is ejected primarily after the main-sequence lifetime of a star is over, which for low and intermediate mass

stars ($m \lesssim 8M_{\odot}$, $t_{\text{life}} \gtrsim 3 \times 10^7$ years) becomes a significant fraction of the relevant timescales (e.g. the 3×10^8 year interval from $z = 6$ to 5).

Neglecting this delay (as in Cen & Chisari 2010) is often justified with the statement that Type II supernova (SNII) yields from short-lived, high-mass stars dominate carbon production at high redshift. However, even if most carbon is synthesised in SNeII⁴, a substantial fraction of that carbon is incorporated into low- and intermediate-mass stars (LIMS, $m \lesssim 8m_{\odot}$) before being blown into the IGM, according to the models of Oppenheimer & Davé (2008). In other words, an important fraction of carbon produced in a galaxy gets locked up in LIMS and is only returned to the gas phase (and made available for ejection in a galactic outflow) during the AGB phase, after the main-sequence lifetime has elapsed. Therefore, the lifetimes of lower-mass stars impose a delay on the ejection of some of the carbon into the IGM, and AGB star ejection of carbon cannot be neglected in calculating the timing of IGM enrichment.

Since we are trying to model the connection between ionizing emission associated with star formation and the eventual enrichment of the IGM with carbon produced by the same stars, it is important that we take this delay into account. Indeed, such a delay is inevitable, and the motivation of this paper was to assess whether this delay might help explain the steep observed evolution of the C IV abundance in the IGM, as discussed in §1.

The cumulative delay function $f_C(t)$ is the fraction of carbon emitted by stars with lifetimes $t_{\text{life}} < t$. Assuming all carbon is ejected at the end of a star's main sequence lifetime, the fraction of carbon ejected in the time interval $t \pm (dt/2)$ after star formation is

$$\frac{df_C}{dt}(t) = \frac{df_C}{dm} \frac{dm}{dt}, \quad (6)$$

where dm/dt is the inverse of the derivative of the lifetime function ($t_{\text{life}}(m)$). The fraction of carbon produced by stars of mass $m \pm (dm/2)$ is

$$\frac{df_C}{dm}(m) \propto M_C(m)\phi(m), \quad (7)$$

where $M_C(m)$ is the carbon mass ejected by a star of mass m , and $\phi(m)$ is the initial mass function (IMF) of stars by number. We normalise this function to give $\int_{t_{\text{min}}}^{t_{\text{max}}} df_C/dt = 1$. Here $t_{\text{min}} = 3.24 \times 10^6$ years is the lifetime of a $100M_{\odot}$ star, and $t_{\text{max}} = 1.52 \times 10^9$ years is the cosmic time between the starting and ending points of our simulations, $z = 100$ and $z = 4.1$. With our chosen IMFs and yields (see below), an additional $< 9\%$ of carbon would emerge at $t > t_{\text{max}}$.

Convoluting the $\Omega_{\text{C IVinst}}(t)$ curve with $\frac{df_C}{dt}$ gives us the delayed C IV curve

$$\Omega_{\text{C IVdelay}}(t) = \Omega_{\text{C IVinst}} * \left(\frac{df_C}{dt} \right). \quad (8)$$

⁴ The fraction of carbon contributed by low and intermediate mass stars depends sensitively on the amount of ‘‘hot bottom burning’’ (HBB) that takes place on the asymptotic giant branch (AGB), since HBB can destroy carbon and even result in a net loss of ^{12}C over the lifetime of a star. The amount of HBB as a function of stellar mass is still highly uncertain, (Ventura & Marigo 2010) so it is unclear whether low- or high-mass stars dominate ^{12}C production (Romano et al. 2010, and references therein).

Romano et al. (2005, 2010) have quantified in detail the impact of uncertainties in the IMF, stellar lifetimes, and stellar yields on Galactic chemical evolution models. The greatest uncertainties are in the yield calculations, which vary considerably from author to author. As Romano et al. (2010) point out, there is no consistent set of yields covering the whole range of mass and metallicity and including all of the physical effects relevant to either galactic or cosmic chemical evolution models, and essentially no suitable calculations have been performed for $m \approx 6 - 8M_{\odot}$. For convenience, we use a set of carbon (^{12}C) yield values provided by Gavián, Buell & Mollá (2005)⁵, containing their own original calculations for $m = 1 - 8M_{\odot}$, and Woosley & Weaver (1995) values for $m = 8 - 100M_{\odot}$. We use the yields for metallicity $Z = 0.02$ because the variation in calculated carbon yield with metallicity (at least above some threshold) is smaller than the overall uncertainty in yields.

The final complication with yields is the distinction between the total mass of an element ejected by a star and the net yield of new atoms synthesised in the star (Gavián et al. 2005). In a self-consistent chemical evolution model that tracks the metallicity of the star-forming environment, the yield of new elements is the relevant quantity. However we are only tracking carbon abundance in the IGM, while stars are forming directly out of gas in the interstellar medium (ISM), so we use the total ejected mass of carbon to calculate the delay. Note that this is independent of the calculation of the total amount of carbon produced (see §3.2). This is a good approximation if the ISM reaches a stable metallicity quickly, and the composition of the galactic outflow is representative of the total mass currently being ejected from stars (both via SN and AGB mass loss).

Theoretical calculations of stellar lifetimes generally agree fairly well for $m > 1M_{\odot}$. The dependence on metallicity is quite weak. The larger uncertainties at $m < 1M_{\odot}$ are irrelevant here since the corresponding lifetime of $t_{\text{life}} > 10$ Gyr is longer than the age of the universe at $z > 0.3$. We adopt the lifetime function of Kodama as given in Romano et al. (2005).

The stellar initial mass function is another important source of uncertainty. We can characterise the impact of the IMF on the delay function by dividing the carbon emission into a prompt component and a delayed component. We are concerned here with evolution on a timescale of $\sim 10^8$ years. Therefore carbon emission that occurs faster than 10^7 years after star formation is relatively prompt. Of the IMFs discussed in the Romano et al. (2005) review, the Kroupa, Tout & Gilmore (1993) and Chabrier (2003) IMFs produce the most extreme values for the cumulative delay function at 10^7 years, $f_C(10^7\text{yr})$. With a Kroupa IMF $f_C(10^7\text{yr}) = 0.23$, while $f_C(10^7\text{yr}) = 0.44$ for a Chabrier IMF. We therefore calculate all of our models with both of these IMFs⁶ in order to demonstrate quantitatively the impact of the IMF uncertainty on our results, and to qualitatively suggest the impact that different sets of yield values

⁵ Available on VizierR: <http://vizier.u-strasbg.fr>

⁶ Note that we are only varying the IMF in the calculation of the delay function. In principal both $\dot{N}/L(1500 \text{ \AA})$ and $r_{\gamma Z}$ depend on the IMF and metallicity of the stellar population, but we treat all of these calculations independently.

might have. Figure 1 shows the differential and cumulative delay functions with Kroupa and Chabrier IMFs. These figures illustrate that roughly half of the carbon ejection occurs essentially instantly, whereas the remaining half is spread over the lifetime ($\sim 1\text{Gyr}$) of intermediate-mass stars.

Extremely low metallicities may result in dramatically different IMFs and yields from those assumed here. We do not consider this metal-free, or Population-III, mode of star formation in calculating the delay function, as metal-free stars are thought to only make up a small fraction of the stars formed before $z = 6$, even if their formation continues at a low rates to late times (see, e.g. Rollinde et al. 2009; Salvaterra et al. 2010).

4 RESULTS

The primary constraints on the epoch of reionization available today are the *WMAP* measurement of τ (the optical depth to Thomson scattering from free electrons in the IGM, Komatsu et al. 2010) and the evolving Lyman- α opacity of the IGM at $z \sim 6$ (though see Mesinger 2010 for a discussion of the complicated, model-dependent interpretation of this evolution). Using the formalism outlined above, we return to the questions posed in the Introduction.

4.1 Matching Reionization Constraints

For our fiducial luminosity function history, we adopt a Schechter luminosity function with fixed ϕ_* and α , and use the observed M_* values from Bouwens et al. (2008) from $z = 3.8$ to 9.0. We extrapolated M_* linearly in z above $z = 9$ with slope β_{M_*} . The extrapolation to lower luminosities is controlled by the faint-end slope, α . Oesch et al. (2009) suggest that M_* is approximately linear in z at high redshift, with a slope of $\beta_{M_*} = 0.36 \pm 0.18$. Bouwens et al. (2008) suggest $\alpha = -1.74$ at high redshift. We use $f_{\text{esc}\gamma} = 0.2$.

Figure 2 shows the ionization and enrichment histories as functions of redshift. The lower (blue) set of curves corresponds to the fiducial parameters described above. The top panel shows the ionized fraction in the IGM, along with the optical depth integrated from redshift 0 to z . The arrows on the right show the total value of the optical depth (integrated to $z = 100$). As Oesch et al. (2009) have pointed out (see also Bolton & Haehnelt 2007), combining this luminosity function evolution with reasonable ionizing photon escape fraction ($f_{\text{esc}\gamma} = 0.2$) and IGM clumping factor ($C = 4$) values, yields an insufficient emissivity to either complete reionization by $z \sim 6$ or match the *WMAP* constraint on the electron scattering optical depth ($\tau = 0.087 \pm 0.014$ Komatsu et al. 2010). With the fiducial LF history, the IGM is only 20% ionized by $z = 6$, and the optical depth is $\tau = 0.036$.

In order to match the *WMAP* τ value and complete reionization at $z \gtrsim 6$, we increase $f_{\text{esc}\gamma} \dot{N}/L(1500 \text{ \AA})$ by a factor of 3, flatten the M_* slope to $\beta_{M_*} = 0.09$, and set the faint end slope to the steeper value of $\alpha = -1.95$. The higher $f_{\text{esc}\gamma} \dot{N}/L(1500 \text{ \AA})$ could be explained by a higher escape fraction, or a higher $\dot{N}/L(1500 \text{ \AA})$ due to a lower metallicity or more top-heavy IMF of the stellar population. For instance, Chary (2008) finds a factor of $\sim 2\text{--}3$ increase in $\dot{N}/L(1500 \text{ \AA})$ when the metallicity falls from $0.4Z_\odot$

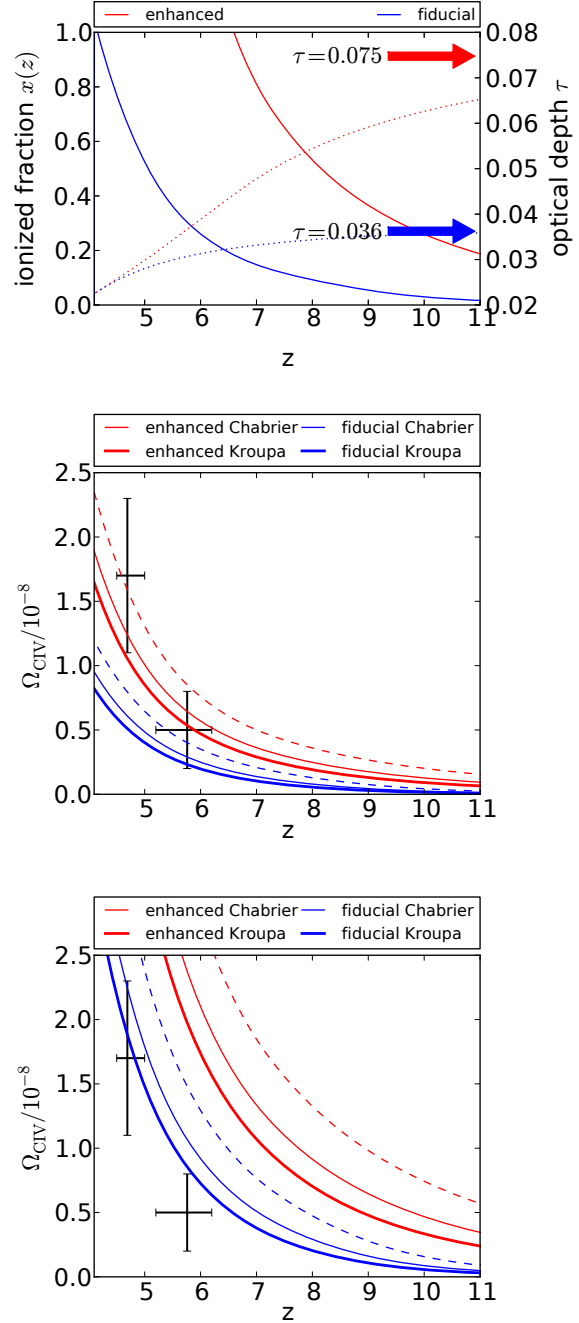


Figure 2. Ionization and enrichment histories of the IGM. In each panel, the lower (blue) set of curves corresponds to the fiducial LF history, and the upper (red) set to the enhanced LF chosen to match *WMAP* $\tau = 0.087$ and $z_{\text{reion}} \sim 6.6$. Top panel: ionized fraction $x(z)$ (solid) and optical depth $\tau(<z)$ (dotted). The arrows on the right show the total value of the optical depth (integrated to $z = 100$). Middle panel: C IV density in the IGM with (solid) and without (dashed) a delay function. The thin solid curve uses the Chabrier-IMF delay, while the thick curve uses the Kroupa-IMF delay. Observed values are indicated as black data points with error bars. Horizontal error bars indicate the interval over which the density is averaged, and vertical error bars indicate the uncertainty. Bottom panel: Enrichment in the same models as in the middle panel, except with $f_{x\text{CIV}}$ increased by a factor of 3.7. This increase is equivalent to the difference between 1/50-solar and solar-metallicity values for the ratio of ionizing photons to metal nucleons.

Table 1. Parameters of our luminosity function (LF) histories.

name	α	β_{M_*}	$f_{\text{esc}\gamma}$	z_{reion}	τ
fiducial	-1.74	0.36	0.2	4.2	0.036
enhanced	-1.95	0.09	0.6	6.6	0.075
<i>WMAP7 (Komatsu et al. 2010):</i>					0.087 \pm 0.014

Parameters:

α is the faint-end slope of the Schechter luminosity function.

β_{M_*} is the slope of M_* as a function of z .

$f_{\text{esc}\gamma}$ is the escape fraction of ionizing photons from galaxies. Note that it is completely degenerate with the SED slope, which we fix at $\dot{N}/L(1500 \text{ \AA}) = 8.4 \times 10^{24} \text{ photons s}^{-1}/(\text{erg s}^{-1} \text{ Hz}^{-1})$.

Results:

z_{reion} is the redshift at which the ionized fraction $x(z) = 1$.

τ is the optical depth due to free electrons.

to $0.02Z_{\odot}$. Note that such changes would affect the delay function and $r_{\gamma Z}$ values as well. The changes to β_{M_*} and α make the enhanced LF history resemble the recent results by Bouwens et al. (2010), who found a brighter M_* and steeper α at $z = 7$ and 8 than were suggested by earlier results. We integrate the LF down to $M_{\text{AB}}(UV) = -13.04$, equivalent to a star formation rate of $0.01 m_{\odot}/\text{yr}$ (Kennicutt 1998; Oesch et al. 2009). Adjusting any of these parameters alone cannot match both constraints, and adjusting them simultaneously allows us to use more plausible values. More important than the exact parameter values is the resulting ionizing emissivity history. This is obviously not a unique solution, but we present this enhanced LF history as a plausible example of one that matches current observational constraints much better than the fiducial extrapolation of the observed LBG luminosity function. The upper (red) sets of curves in Figure 2 correspond to this enhanced LF history. The top panel shows that the optical depth has been increased to near the *WMAP* value, and the IGM is fully ionized by $z = 6.6$. Table 1 summarises the parameters of each LF history.

We use a constant clumping factor $C = 4$ in these calculations, though our basic conclusion that the enhanced LF history is consistent with existing reionization constraints is not particularly sensitive to changes in this assumption. For instance, using a higher constant $C = 6$ results in $\tau = 0.067$, $z_{\text{reion}} = 6.21$ for the enhanced LF history. The clumping factor should actually be lower at higher redshift, however. Chary (2008) has derived the clumping factor as a function of redshift for the relevant gas (ionized gas outside of ionizing-photon source halos) from simulations by Trac & Cen (2007). Using their clumping factor history (estimated from their Figure 2a), results in a larger $\tau = 0.082$ quite close to the *WMAP7* values (because the clumping factor is lower, $C < 4$, at early times, $z > 10.5$) and a later $z_{\text{reion}} = 5.7$ (because $C \gtrsim 8$ at $z \lesssim 7$). Pawlik, Schaye & van Scherpenzeel (2009b,a) found that reheating of the IGM results in an even lower clumping factor history, which might require slightly less enhancement in the LF history to match reionization constraints.

4.2 Matching CIV Abundance

The bottom two panels of Figure 2 display the CIV mass density as a fraction of the critical density $\Omega_{\text{CIV}}(z)$. The dashed lines assume instantaneous ejection, the thin solid lines are convolved with the Chabrier-IMF-based delay function, and the thick solid lines with the longer Kroupa-IMF delay.

In order to show the effect of the large uncertainty in the value of $f_{x\text{CIV}}$, in the middle panel we use the $1/50 Z_{\odot}$ value for $f_{x\text{CIV}}$, while in the bottom panel with use the solar-metallicity value (see §3.2). The solar-metallicity stellar population produces fewer ionizing photons per metal nucleon synthesised, so for a fixed LF history it produces higher Ω_{CIV} values. Both of the puzzles discussed in §1 are evident in the middle panel, which effectively uses the same $f_{x\text{CIV}}$ assumed by Ryan-Weber et al. (2009).

In particular, first, we can see the conflict suggested by Ryan-Weber et al. (2009) between reionization constraints and the low $z = 5.8$ Ω_{CIV} value in the middle panel of Figure 2. The enrichment history calculated from the LF history that matches reionization constraints (upper/red dashed curve) produces too much CIV at $z = 5.8$.⁷ This overproduction at a single redshift, in and of itself, is not too troubling. Either a slight decrease in the highly-uncertain $f_{x\text{CIV}}$ or a slight decrease in the SFRD could lower Ω_{CIV} sufficiently to agree with the $z = 5.8$ measurement. Also, the stellar-lifetime delay, especially with the less top-heavy Kroupa IMF, brings Ω_{CIV} down to close to the observed value.

The second puzzle — the rapid buildup of CIV from $z = 5.8$ to 4.7 noted by Becker et al. (2009) — is also evident. In the middle panel, again, the enhanced LF curve with no delay is close to matching the $z = 4.7$ observation, but slightly over-predicts the earlier $z = 5.8$ point. Similarly, the fiducial LF curve with no delay only slightly under-predicts the $z = 5.8$ value, but is much lower than the later $z = 4.7$ observation. The predicted evolution of Ω_{CIV} using either LF history is too slow to match the observations.

We were motivated to calculate the stellar-lifetime-based enrichment delay by the idea that such a delay might help to explain to rapid rise in CIV. In fact, as Figure 2 clearly illustrates, we find that the delay contributes little to the solution of this puzzle. In the next subsection, we explore the effect of longer delays.

4.3 The Rapid Rise in CIV

Since $f_{x\text{CIV}}$ is so uncertain, it is useful to find a quantity independent of $f_{x\text{CIV}}$ to compare with the observations. For a given combination of an ionizing emissivity history and a delay function, the fractional increase in Ω_{CIV} over a specific redshift interval is fixed and does not depend on $f_{x\text{CIV}}$ (as long as $f_{x\text{CIV}}$ is independent of redshift). The observed fractional increase is

$$\frac{\Delta\Omega_{\text{CIV}}}{\Omega_{\text{CIV}}} \equiv \frac{\Omega_{\text{CIV}}(4.7)}{\Omega_{\text{CIV}}(5.8)} - 1 = 2.4. \quad (9)$$

⁷ Again, we are ignoring the large errors on the observations for the sake of exploring their consequences should they prove to be accurate.

To compare this number with our theoretical curves, we average Ω_{CIV} over the same intervals used to determine the observed values. With no delay, the fractional increase is $\Delta\Omega_{\text{CIV}}/\Omega_{\text{CIV}} = 0.79$ for the fiducial LF history, and 0.70 for the enhanced LF history. These values are far smaller than the observed increase.

We expect a delay in enrichment to make the fractional increase in C IV larger, because (if Ω_{CIV} evolves slower than exponentially) the fractional rate of increase at earlier times must be higher. To show this, consider that the fractional increase is roughly

$$\frac{\Delta\Omega_{\text{CIV}}}{\Omega_{\text{CIV}}} \approx \frac{\dot{\Omega}_{\text{CIV}}}{\Omega_{\text{CIV}}}(t)\Delta t, \quad (10)$$

where $\Delta t \sim 0.3$ Gyr is the time interval from $z = 5.8$ – 4.7 and $\dot{\Omega}_{\text{CIV}}$ is the derivative of Ω_{CIV} with respect to cosmic time. If Ω_{CIV} is a power-law, proportional to t^n (this is a reasonable approximation at the cosmic times we are considering, and it is also a conservative one, in the sense that structure formation is increasingly more rapid at higher redshifts), then

$$\frac{\dot{\Omega}_{\text{CIV}}}{\Omega_{\text{CIV}}}(t) = \frac{n}{t}. \quad (11)$$

Therefore, the fractional growth rate decreases with time. If we had a delta-function delay, so that $\Omega_{\text{CIVdelay}}(t) = \Omega_{\text{CIVinst}}(t - t_{\text{delay}})$, then the delay would boost the fractional increase by a factor of

$$\frac{\dot{\Omega}_{\text{CIVdelay}}/\Omega_{\text{CIVdelay}}}{\dot{\Omega}_{\text{CIVinst}}/\Omega_{\text{CIVinst}}} \sim \frac{t}{t - t_{\text{delay}}}. \quad (12)$$

We need a factor of $t/(t - t_{\text{delay}}) = 3$ – 3.5 to boost the fractional C IV increase from $\Delta\Omega_{\text{CIV}}/\Omega_{\text{CIV}} = 0.7$ – 0.8 to 2.4. We can conclude that a delta-function delay of ~ 0.7 Gyr should boost the growth sufficiently to match the slope inferred from the two observations. Our stellar-lifetime-based delays, however, are too short to provide the necessary boost. The mean delay with the Chabrier IMF is 0.16 Gyr. With the Kroupa IMF, the mean delay is only slightly longer, 0.25 Gyr. Furthermore, and even more problematically, the delay is not a delta function. A large fraction (roughly half; see Figure 1) of the carbon is ejected promptly, which dilutes the boosting effect.

Figure 3 shows enrichment histories with $f_{x\text{CIV}}$ adjusted to fit $\Omega_{\text{CIV}}(z = 4.7)$ to the observed value. This allows us to assess the effect of the delay on the slope by comparing the earlier evolution of the Ω_{CIV} curve to the observed value at $z = 5.8$. If C IV absorber production is too slow, $\Delta\Omega_{\text{CIV}}/\Omega_{\text{CIV}}$ will be too small, and we will over-predict the earlier measurement. Table 2 gives the $f_{x\text{CIV}}$ and $\Delta\Omega_{\text{CIV}}/\Omega_{\text{CIV}}$ values for each combination of LF history and delay function.

The stellar-lifetime delays are insufficient to boost the C IV growth to the observed rate, whereas assuming a 0.7 Gyr delay instead brings the enhanced LF history into agreement with the observations (top panel of Figure 3). Since the stellar lifetime delay is inevitable, even if a longer delay is also in effect, we next add the 0.7 Gyr delay to the stellar-lifetime-based delay (middle panel of Figure 3). When the stellar lifetime delays are added, the fractional growth is increased by 25–50% (for the Chabrier and Kroupa delays, respectively). In the bottom panel of Figure 3 we add

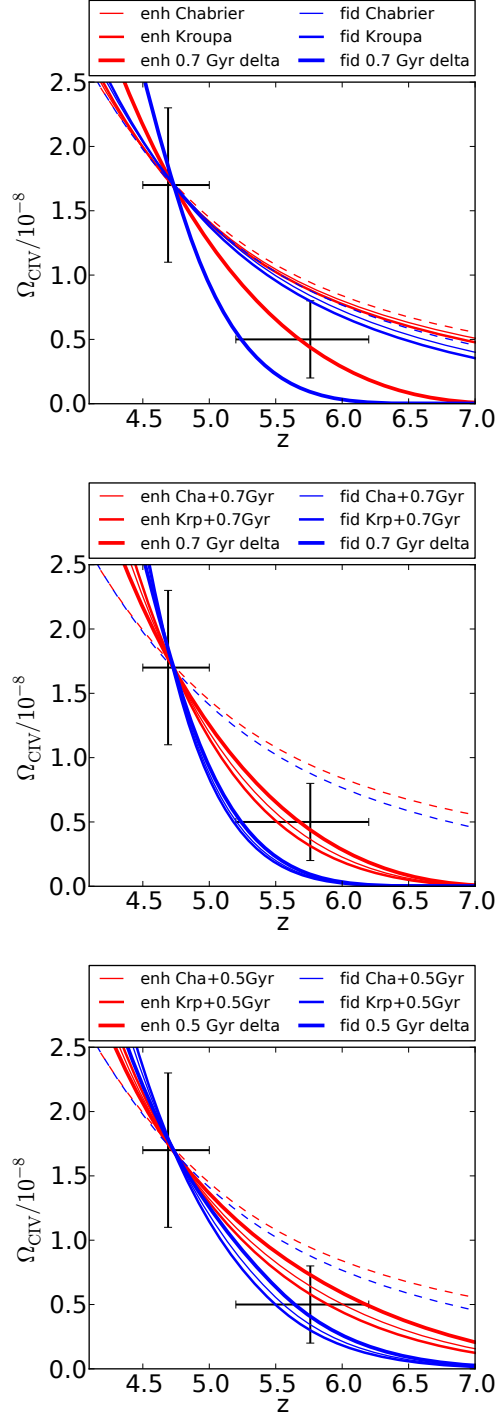


Figure 3. Enrichment histories with the stellar carbon-to-ionizing-photon production ratio, $f_{x\text{CIV}}$, adjusted to match the $z = 4.7$ observation. The dashed curves assume instantaneous production of C IV. Top panel: comparing stellar-lifetime based delays and a 0.7 Gyr delta function delay. Middle panel: a 0.7 Gyr delay has been added to the stellar-lifetime delays. Bottom panel: a 0.5 Gyr delay has been added to stellar-lifetime delays.

Table 2. Fractional increase in C IV density for each luminosity function history and delay function combination.

LF History	Delay Function (1)	$f_{xCIV}/10^{-9}$ (2)	$\Delta\Omega_{CIV}/\Omega_{CIV}$ (3)
<i>observed Ω_{CIV} evolution</i>		—	2.4
enhanced	no delay	1.5	0.7
enhanced	Chabrier	1.9	0.7
enhanced	Kroupa	2.3	0.8
enhanced	0.5 Gyr delta	4.5	1.1
enhanced	Cha + 0.5 Gyr	6.2	1.3
enhanced	Krp + 0.5 Gyr	7.8	1.5
enhanced	0.6 Gyr delta	5.9	1.4
enhanced	Cha + 0.6 Gyr	8.4	1.8
enhanced	Krp + 0.6 Gyr	10.7	2.1
enhanced	0.7 Gyr delta	7.9	2.1
enhanced	Cha + 0.7 Gyr	11.8	2.6
enhanced	Krp + 0.7 Gyr	15.7	3.1
fiducial	no delay	3.0	0.8
fiducial	Chabrier	3.9	0.9
fiducial	Kroupa	4.7	1.0
fiducial	0.5 Gyr delta	10.8	2.3
fiducial	Cha + 0.5 Gyr	16.3	2.7
fiducial	Krp + 0.5 Gyr	21.7	3.2
fiducial	0.6 Gyr delta	15.6	4.0
fiducial	Cha + 0.6 Gyr	24.7	4.8
fiducial	Krp + 0.6 Gyr	34.6	5.4
fiducial	0.7 Gyr delta	25.4	8.2
fiducial	Cha + 0.7 Gyr	42.7	9.5
fiducial	Krp + 0.7 Gyr	62.5	10.5

(1) Figure 3 shows the corresponding enrichment history for each row in this table (except the 0.6 Gyr delays).

(2) The f_{xCIV} value given is the one needed to match Ω_{CIV} at $z = 4.7$. Compare to our estimates of $f_{xCIV} = 1.4 \times 10^{-9}$ for $Z = 1/50 Z_{\odot}$, or 5.0×10^{-9} for $Z = Z_{\odot}$.

(3) $\Delta\Omega_{CIV}/\Omega_{CIV}$ is independent of f_{xCIV} .

a shorter 0.5 Gyr delay. Table 2 also includes an intermediate 0.6 Gyr additional delay.

The stellar-lifetime delays have an effect on both the length of the additional delay and the f_{xCIV} value needed to match the observations. For instance, with the enhanced LF history and a delta function delay of 0.7 Gyr, the fractional increase is 2.1 and $f_{xCIV} = 7.9 \times 10^{-9}$. With the Kroupa-IMF delay included, an shorter additional delay of 0.6 Gyr produces the same fractional increase, but then f_{xCIV} must be increased by 35%. Therefore, future models designed to study the relationships between reionization, enrichment, and galaxy formation must include the finite stellar lifetimes in order to draw precise quantitative conclusions.

While some of the f_{xCIV} values in Table 2 are physically plausible, some may be unphysically high, indicating that certain delay function and LF history combinations are not reasonable candidates for explaining the observed evolution. For instance, the fiducial LF with a delta-function delay of 0.7 Gyr requires the rather high value of $f_{xCIV} = 2.5 \times 10^{-8}$. On the other hand, $f_{xCIV} = 7.9 \times 10^{-9}$ (for the enhanced LF history with 0.7 Gyr delay function delay) could plausibly be explained as the result of a solar-metallicity $r_{\gamma Z}$ (ionizing

photon to metal nucleon ratio) and $f_{escZ} = 0.3$ (instead of 0.2).

In Table 2 and Figure 3 we have shown that, without any change in the C IV ionization correction, a ~ 0.5 – 0.7 Gyr delay between the production of ionizing photons and C IV absorption features can explain the rapid increase in C IV density between $z = 5.8$ and 4.7 . Simulations (Oppenheimer et al. 2009; Cen & Chisari 2010) suggest that the triply-ionized fraction of carbon may increase by a factor of up to 1.25 in this interval, which would help to explain the observed rise, but would leave a factor of $\gtrsim 2.7$ increase ($\Delta\Omega_C/\Omega_C = 1.7$) in the total carbon content of the IGM. Equation 12 and Table 2 tell us that this growth still requires a delay of 0.6 Gyr with the enhanced LF history, or (not shown in the table) ~ 0.4 Gyr for the fiducial LF.

Since stellar lifetimes were too short to provide the required delay, what mechanism could explain a longer ~ 0.5 – 0.7 Gyr timescale? One option would be to change the stellar IMF. However, this would require making the IMF radically more bottom-heavy at high redshift (in fact, it must essentially be truncated at a few solar masses to produce the required delay) — in opposition to the trend expected for stars forming from metal-poor gas. Alternatively, we may posit that carbon ejected from a galaxy must reach a characteristic distance before producing a C IV absorption feature visible in current data sets. In this case, the relevant timescale would be approximately the ratio of the distance and the mean outflow velocity. The distance from the source galaxy at which C IV is observed can be affected both by the ionization state of the carbon as a function of distance, and the filling factor of observable C IV absorbers. If the volume-filling factor of the absorbers is too low, absorption systems will become too rare for detection in the limited set of sight lines currently available.

Numerical simulations seem to suggest that both ionization and filling-factor effects are at work. Oppenheimer et al. (2009) find that C IV absorbers at $z = 6$ tend to have left their source galaxy 0.1–0.5 Gyr earlier, and lie within 10–50 kpc of a galaxy in their simulation (giving average speeds of ~ 30 – 300 km/s). They find that photo-ionization dominates the production of C IV, and suggest that the ionizing radiation from the source galaxy largely determines the distance at which carbon is seen as C IV. Cen & Chisari (2010) found absorbers at similar distances (~ 70 kpc). In their simulations, collisional ionization is important to the C IV ionization balance, and they suggest that at least some C IV absorbers are produced in shocks formed in galactic outflows. Oppenheimer et al. (2009) also find that, as metals travel farther from the source galaxy, they enrich less dense regions of the IGM and produce weaker C IV absorption systems. Therefore (neglecting the ionization effects for the moment) absorbers near a galaxy will have a higher column density, but a smaller filling factor (and will therefore be detected more rarely), while absorbers farther from the galaxy will have a lower column densities, but larger filling factors. Whatever is determining the distance scale, a ~ 0.5 – 0.7 Gyr delay could naturally be explained as the result of a ~ 100 km/s outflow carrying carbon to a distance of ~ 50 – 70 kpc before it is seen in C IV absorption.

If the filling-factor evolution dominates the delay, it leads to an interesting prediction: if the C IV has indeed al-

ready been ejected from galaxies, and the reason it is not yet seen at the highest redshifts is that it has not yet spread to occupy a detectable filling factor, then future observations, with significantly larger effective lines-of-sight, could uncover much of this hitherto hidden carbon in rare, high-column density C IV absorbers.⁸ This could confirm, in principle, that the total amount of carbon present in the IGM tracks the cosmic star-formation history, but the rise in the filling factor of C IV is driven on a longer timescale, determined by the finite (relatively low) speed of the carbon-transporting winds.

5 DISCUSSION

We have shown that a ~ 0.5 – 0.7 Gyr delay between the production of ionizing photons and C IV absorption features can explain the rapid evolution of the C IV density in the IGM between $z = 5.8$ and 4.7 . No change in the ratio of carbon to ionizing photon production (the ionizing efficiency) or in the ionization correction for C IV is required. Evolution in the ionization correction could lower the required delay to ~ 0.4 – 0.6 Gyr. This delay has a natural physical explanation, namely the need to transport carbon a certain distance into the IGM before it is seen in C IV absorption. The distance scale would be determined by a combination of the need to enrich a sufficient volume of the IGM to be detectable in a limited number of quasar sight lines, and possible ionization effects that optimise the C IV fraction at a certain distance from the source galaxy. An outflow of 100 km s^{-1} would carry material to a distance of 40 – 70 kpc in this timescale.

The shorter delay due to finite stellar lifetimes cannot provide the full explanation for the rapid evolution, but must be included in future models in order to properly understand the relationships between galaxy formation, reionization, and enrichment of the IGM.

Future measurements of metal abundance in the IGM will provide important constraints on these relationships. Perhaps the most important improvement will come from probing more quasar lines of sight, both to reduce the uncertainty in the density of absorbers in the currently-detected column-density range ($10^{13.5}$ – $10^{14.5}$; Ryan-Weber et al. 2009), and to search for the rare, high-column-density absorbers that we expect to exist close to galaxies. This does not require a high resolution or signal-to-noise ratio (Oppenheimer et al. 2009), just the identification of more high- z quasars and the taking of their near-IR absorption spectra (though probing the weak end of the column-density distribution will require higher quality spectra). The Multi Unit Spectroscopic Explorer (MUSE; Bacon et al. 2006), an integral field unit for the VLT, will be ideal for directly exploring the relationship between galaxies and IGM absorbers because it will be able to simultaneously obtain spectroscopic redshifts for large numbers of galaxies (up to $z \sim 6.6$) near a quasar line of sight, which can then

be compared with the redshift distribution of absorbers seen in the quasar spectrum.

Observations of multiple ionization stages of several elements, using the sensitivity and wavelength coverage of new and future near-IR spectrographs like X-shooter, will break the degeneracy of the factors entering into $f_{x\text{-CIV}}$, since some factors should be (approximately) independent of element (such as $f_{\text{esc}Z}$ and $r_{\gamma Z}$), while the fraction of carbon in the C IV stage (f_{CIV}) can be constrained from measurements of the ionization balance in other species (Ryan-Weber et al. 2009). Detailed physical models will be crucial in interpreting these future observations. Such work is already underway (Oppenheimer et al. 2009; Cen & Chisari 2010), but needs to be improved to model both reionization and enrichment self-consistently.

6 ACKNOWLEDGEMENTS

We would like to thank Francesca Matteucci for discussion of stellar chemical yields. ZH acknowledges financial support by the Polányi Program of the Hungarian National Office for Research and Technology (NKTH). RHK is supported by a Zwicky Fellowship at ETH Zurich. PM would like to acknowledge NSF grant AST-0908910.

This work made use of the COSMOLOGY package⁹, version 0.1, and the VizieR database of astronomical catalogues¹⁰ (Ochsenbein, Bauer & Marcout 2000).

REFERENCES

- Asplund M., Grevesse N., Sauval A. J., 2005, in T. G. Barnes III & F. N. Bash ed., *Cosmic Abundances as Records of Stellar Evolution and Nucleosynthesis Vol. 336 of Astronomical Society of the Pacific Conference Series, The Solar Chemical Composition*. pp 25–+
- Bacon R., et al., 2006, *The Messenger*, 124, 5, arXiv:astro-ph/0606329
- Becker G. D., Rauch M., Sargent W. L. W., 2009, *ApJ*, 698, 1010, arXiv:0812.2856
- Bolton J. S., Haehnelt M. G., 2007, *MNRAS*, 382, 325, arXiv:astro-ph/0703306
- Bouwens R. J., Illingworth G. D., Franx M., Ford H., 2007, *ApJ*, 670, 928, arXiv:0707.2080
- Bouwens R. J., Illingworth G. D., Franx M., Ford H., 2008, *ApJ*, 686, 230, arXiv:0803.0548
- Bouwens R. J., Illingworth G. D., Oesch P. A., Labbe I., Trenti M., van Dokkum P., Franx M., Stiavelli M., Carollo C. M., Magee D., Gonzalez V., 2010, *ArXiv e-prints*, arXiv:1006.4360
- Cen R., Chisari N. E., 2010, *ArXiv e-prints*, arXiv:1005.1451
- Chabrier G., 2003, *PASP*, 115, 763, arXiv:astro-ph/0304382
- Chary R., 2008, *ApJ*, 680, 32, arXiv:0712.1498
- Davé R., Oppenheimer B. D., 2007, *MNRAS*, 374, 427, arXiv:astro-ph/0608268

⁸ The lack of detection of weak C IV absorbers in the Becker et al. (2009) observations is evidence against the alternative hypothesis that the carbon is hidden in systems too weak to detect with the quality of spectra currently available.

⁹ <http://roban.github.com/CosmoLoPy/>

¹⁰ <http://vizier.u-strasbg.fr/>

- Gavilán M., Buell J. F., Mollá M., 2005, *A&A*, 432, 861, arXiv:astro-ph/0411746
- Hui L., Gnedin N. Y., 1997, *MNRAS*, 292, 27, arXiv:astro-ph/9612232
- Kennicutt Jr. R. C., 1998, *ARA&A*, 36, 189, arXiv:astro-ph/9807187
- Komatsu E., et al., 2010, *ArXiv e-prints*, arXiv:1001.4538
- Kroupa P., Tout C. A., Gilmore G., 1993, *MNRAS*, 262, 545
- Mesinger A., 2010, *MNRAS*, pp 1017–+, arXiv:0910.4161
- Ochsenbein F., Bauer P., Marcout J., 2000, *A&AS*, 143, 23, arXiv:astro-ph/0002122
- Oesch P. A., Carollo C. M., Stiavelli M., Trenti M., Bergeron L. E., Koekemoer A. M., Lucas R. A., Pavlovsky C. M., Beckwith S. V. W., Dahlen T., Ferguson H. C., Gardner J. P., Lilly S. J., Mobasher B., Panagia N., 2009, *ApJ*, 690, 1350, arXiv:0804.4874
- Oppenheimer B. D., Davé R., 2006, *MNRAS*, 373, 1265, arXiv:astro-ph/0605651
- Oppenheimer B. D., Davé R., 2008, *MNRAS*, 387, 577, arXiv:0712.1827
- Oppenheimer B. D., Davé R., Finlator K., 2009, *MNRAS*, 396, 729, arXiv:0901.0286
- Pawlik A. H., Schaye J., van Scherpenzeel E., 2009a, *ArXiv e-prints*, arXiv:0912.3034
- Pawlik A. H., Schaye J., van Scherpenzeel E., 2009b, *MNRAS*, 394, 1812, arXiv:0807.3963
- Pettini M., Madau P., Bolte M., Prochaska J. X., Ellison S. L., Fan X., 2003, *ApJ*, 594, 695, arXiv:astro-ph/0305413
- Rollinde E., Vangioni E., Maurin D., Olive K. A., Daigne F., Silk J., Vincent F. H., 2009, *MNRAS*, 398, 1782, arXiv:0806.2663
- Romano D., Chiappini C., Matteucci F., Tosi M., 2005, *A&A*, 430, 491
- Romano D., Karakas A. I., Tosi M., Matteucci F., 2010, *ArXiv e-prints*, arXiv:1006.5863
- Ryan-Weber E. V., Pettini M., Madau P., Zych B. J., 2009, *MNRAS*, 395, 1476, arXiv:0902.1991
- Salvaterra R., Ferrara A., Dayal P., 2010, *ArXiv e-prints*, arXiv:1003.3873
- Schaerer D., 2002, *A&A*, 382, 28, arXiv:astro-ph/0110697
- Songaila A., 2001, *ApJ*, 561, L153, arXiv:astro-ph/0110123
- Tilvi V., Rhoads J. E., Hibon P., Malhotra S., Wang J., Veilleux S., Swaters R., Probst R., Krug H., Finkelstein S. L., Dickinson M., 2010, *ArXiv e-prints*, arXiv:1006.3071
- Trac H., Cen R., 2007, *ApJ*, 671, 1, arXiv:astro-ph/0612406
- Tyson N. D., 1988, *ApJ*, 329, L57
- Ventura P., Marigo P., 2010, *ArXiv e-prints*, arXiv:1007.2533
- Woosley S. E., Weaver T. A., 1995, *ApJS*, 101, 181